Struct Multidisc Optim (2014) 50:453–464
DOI 10.1007/s00158-014-1064-4

RESEARCH PAPER

Piezoresistive device optimization using topological derivative concepts

S. M. Giusti · L. A. M. Mello · E. C. N. Silva

Received: 26 May 2013 / Revised: 31 December 2013 / Accepted: 6 February 2014 / Published online: 6 June 2014

Abstract A piezoresistive sensor is composed of a piezoresistive membrane attached to a flexible plate. The piezoresistive material is anisotropic, and its electrical properties change when subjected to mechanical stresses. In this work, the topology design of a piezoresistive pressure sensor is addressed. More specifically, an optimization technique based on topological sensitivity analysis is proposed in order to obtain the optimized distribution of piezoresistive material over the plate. In most of the works regarding topological sensitivity analysis, isotropic materials are considered. However, the problem of conductivity in an anisotropic non-homogeneous domain has been recently addressed, and a closed form for the topological derivative associated to the energy shape functional has been presented. In this work, on the other hand, a closed form for the topological derivative associated with a multi-objective shape functional related to the steady-state anisotropic current density diffusion problem is presented. To illustrate the applicability of the closed formula and the proposed optimization procedure, numerical examples regarding the conceptual design of piezoresistive sensors, considering distinct optimization parameters and boundary conditions in the conductivity problem, are presented.

Keywords Topological derivative · Topological design · Finite element method · Piezoresistive pressure sensor

S. M. Giusti
Departamento de Ingeniería Civil, Facultad Regional Córdoba, Universidad Tecnológica Nacional (UTN/FRC - CONICET), Maestro M. López esq. Cruz Roja Argentina, X5016ZAA Córdoba, Argentina
e-mail: sgiusti@civil.frc.utn.edu.ar

L. A. M. Mello · E. C. N. Silva (✉)
Department of Mechatronics and Mechanical Systems Engineering, School of Engineering, University of São Paulo, 05508-030 São Paulo, Brazil
e-mail: ecnsilva@usp.br

L. A. M. Mello
e-mail: luis.mello@usp.br

1 Introduction

A piezoresistive sensor is composed of a piezoresistive membrane attached to a flexible plate (substrate), see Fig. 1. This membrane is composed by a material whose electrical properties change when subjected to mechanical stresses or when internal damage initiates or propagates. In fact, when an external load is applied over the plate, the strain over the top (or bottom) face of the plate is induced to the piezoresistive membrane. Under this applied strain the material reacts developing a mechanical stress state and, as consequence, a change in the conductivity property appears. Piezoresistive sensor modeling has been extensively discussed in the literature (see Sze (2000), Buchhold et al. (2000), Plaza et al. (2000, 2002) Hsieh et al. (2001), for instance). Piezoresistive sensors are used in several applications, such as inclinometers (Mescheder and Majer 1997), pressure sensors (Buchhold et al. 2000), accelerometers (Plaza et al. 2000; Amarasinghe et al. 2005), and atomic force microscope probes (Pedersen 2004). In this work, the topology design of a pressure sensor is addressed. More specifically, we apply an optimization technique based on topological sensitivity analysis in order to obtain the optimized distribution of piezoresistive material over the plate.

According to the literature about topological sensitivity analysis, theoretical developments and its application are oriented to study problems with isotropic constitutive

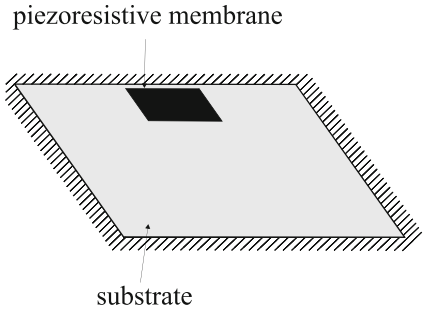

Fig. 1 Schematics of a piezoresistive pressure sensor

behavior of the material. Only a few works discuss the problem of non-isotropic constitutive behavior. In fact, the problem of conductivity in an orthotropic domain is studied in the work by Sokołowski and Żochowski (1999) and their presented result is extended by Giusti et al. (2010a). The problem of conductivity in an anisotropic non-homogeneous domain is treated recently by Giusti and Novotny (2012), where a closed form for the topological derivative associated to the energy shape functional is presented. In this work, we use a closed form for the topological derivative associated to a multi-objective shape functional in the conceptual design of piezoresistive pressure sensors.

The optimized design of piezoresistive sensors has been discussed in the literature, see the works by Pedersen (2004), Rubio et al. (2008) and Mello et al. (2012), for instance. The approach proposed in this work belongs to the methods based on the level-set domain representation (Wang et al. 2003, 2011; Amstutz 2006).

This paper is organized as follows. Section 2 describes the model associated to the anisotropic current density diffusion problem. The mathematical concepts associated to the topological sensitivity analysis and the topological derivative are introduced in Section 3. The topological optimization procedure associated to the problem under consideration is presented in Section 4, where we present a complete and detailed methodology for the topology design of piezoresistive membranes attached to a flexible plate. In Section 5, four numerical experiments concerning the optimized design of piezoresistive pressure sensors are presented. The paper ends in Section 6 where concluding remarks are presented.

2 Formulation of the piezoresistive problem

In this Section, the weak formulation regarding the differential equations that govern the electrical behavior of a piezoresistive membrane is provided, together with the conductivity tensor of a piezoresistive material. In this work, it is assumed that the flexible substrate is metallic and that it is grounded, as carried out by Rubio et al. (2008) and by Mello et al. (2012), and thus, only its structural response must be computed. As already mentioned, a piezoresistive sensor consists of a piezoresistive membrane deposited onto a flexible substrate. Therefore, we assume that the structural model of the sensor is composed of a Kirchhoff plate coupled to a two-dimensional piezoresistive membrane. Piezoresistive sensor modeling has been extensively discussed in the literature (see Buchhold et al. (2000), Plaza et al. (2000, 2002), Hsieh et al. (2001), Pedersen (2004), Rubio et al. (2008) and Mello et al. (2012), for instance). Authors refer to the work by Mello et al. (2012) for the constitutive equations regarding loaded and unloaded piezoresistive sensors, and for the strong formulation of a piezoresistive sensor, which encompasses differential equations for the structural and electrical behaviors.

For the unloaded sensor, φ is solution of the following general variational problem: find the electric field $\varphi \in \mathcal{U}$, such that

$$\int_\Omega K\nabla\varphi \cdot \nabla\eta \, d\Omega = 0 \qquad \forall \eta \in \mathcal{V} \,, \tag{1}$$

where K is the symmetric second order conductivity tensor. For the case of isotropic constitutive behavior, the second-order conductivity tensor K admits the representation $K = kI$, with k being the conductivity coefficient (scalar value) and I is the identity tensor of second order. In the variational problem (1) the set of admissible electric fields $\mathcal{U}$, and the space of admissible virtual electric fields $\mathcal{V}$, are given by

$$\begin{aligned} \mathcal{U} &:= \left\{ \xi \in H^1(\Omega) : \xi|_{\Gamma_D} = \bar{\varphi} \right\} \quad \text{and} \\ \mathcal{V} &:= \left\{ \xi \in H^1(\Omega) : \xi|_{\Gamma_D} = 0 \right\}. \end{aligned} \tag{2}$$

In addition, $\partial\Omega$ is used to denote the boundary of the domain Ω and $\partial\Omega = \overline{\Gamma_N \cup \Gamma_D}$ with $\Gamma_N \cap \Gamma_D = \varnothing$, where Γ_N and Γ_D are Neumann and Dirichlet boundaries, respectively. Thus, $\bar{\varphi}$ is a Dirichlet data on Γ_D that is assumed to be smooth enough, see Fig. 2 (note that homogeneous Neumann boundary conditions on Γ_N are considered).

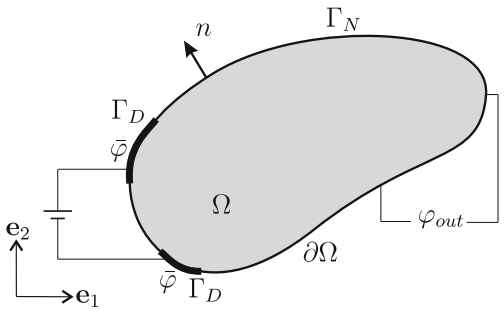

Fig. 2 Formulation of the piezoresistive problem

When a system of external forces is applied to the plate (or substrate) the conductivity of the piezoresistive membrane changes with the mechanical stress acting over the surface where the membrane is attached. Then, for the loaded device, ϕ is the solution of the following variational problem: find the electric field $\phi \in \mathcal{U}$, such that

$$\int_\Omega \bar{K}\nabla\phi \cdot \nabla\eta \, d\Omega = 0 \qquad \forall \eta \in \mathcal{V} \,, \tag{3}$$

where $\bar{K} = \bar{K}(x)$ is a symmetric second order conductivity tensor, given by

$$\begin{aligned} \bar{K} &= k \left\{ \begin{Bmatrix} 1 \\ 1 \\ 1 \\ 0 \\ 0 \\ 0 \end{Bmatrix} - \begin{bmatrix} \pi_{11} & \pi_{12} & \pi_{12} & 0 & 0 & 0 \\ \pi_{12} & \pi_{11} & \pi_{12} & 0 & 0 & 0 \\ \pi_{12} & \pi_{12} & \pi_{22} & 0 & 0 & 0 \\ 0 & 0 & 0 & \pi_{44} & 0 & 0 \\ 0 & 0 & 0 & 0 & \pi_{44} & 0 \\ 0 & 0 & 0 & 0 & 0 & \pi_{44} \end{bmatrix} \begin{Bmatrix} \sigma_x \\ \sigma_y \\ \sigma_z \\ \sigma_{yz} \\ \sigma_{xz} \\ \sigma_{xy} \end{Bmatrix} \right\} \\ &= K(I - \pi\sigma) \,, \end{aligned} \tag{4}$$

being π the piezoresistive constitutive property tensor and $\sigma = \mathbb{C}\varepsilon$ is the stress tensor on the piezoresistive membrane. Notice that the elasticity tensor $\mathbb{C}$ is an orthotropic tensor in the case of piezoresistive materials and ε is strain on the membrane, induced by the strain of the plate. For a detailed explanation on the derivation of the constitutive behavior, we refer the reader to the works by Xiao et al. (1999), Buchhold et al. (2000) and Mello et al. (2012).

3 Topological derivative concept

The topological sensitivity analysis gives the topological asymptotic expansion of a shape functional with respect to an infinitesimal singular domain perturbation. The main term of this expansion is a scalar field called topological derivative. In order to introduce these concepts, let us consider an open bounded domain $\Omega \subset \mathbb{R}^2$, which is subjected to a non-smooth perturbation in a small region $B_\rho(\widehat{x})$ of size ρ with center at an arbitrary point $\widehat{x} \in \Omega$. Thus, introducing a characteristic function $\chi = \mathbb{1}_\Omega$, associated to the unperturbed domain, it is possible to define the characteristic function associated to the topological perturbed domain χ_ρ. Particularly, if the topological perturbation is a inclusion, we have $\chi_\rho(\widehat{x}) = \mathbb{1}_\Omega - (1-\gamma)\mathbb{1}_{\overline{B_\rho(\widehat{x})}}$, where $\gamma \in \mathbb{R}^+$ is the contrast parameter in the material property of the medium, see Fig. 3. Then we assume that a given shape functional $\psi(\chi_\rho(\widehat{x}))$, associated to the topological perturbed domain, admits the following topological asymptotic expansion

$$\psi(\chi_\rho(\widehat{x})) = \psi(\chi) + f(\rho) T_D\psi(\widehat{x}) + o(f(\rho)) \,, \tag{5}$$

where $\psi(\chi)$ is the shape functional associated to the unperturbed domain, $f(\rho)$ is a function such that $f(\rho) \to 0^+$,

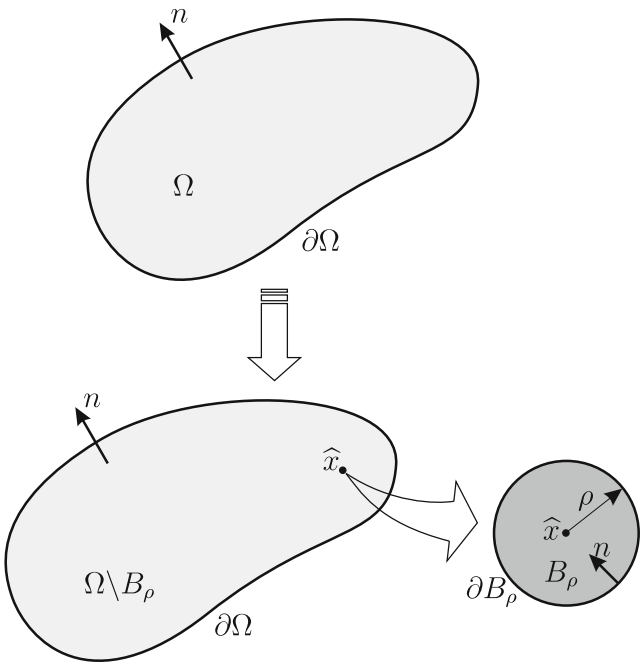

Fig. 3 Topological derivative concept

with $\rho \to 0$. A function $\widehat{x} \mapsto T_D\psi(\widehat{x})$ is the so-called topological derivative of ψ in the point $\widehat{x}$. Thus, the topological derivative can be seen as a first order correction factor over $\psi(\chi)$ to approximate $\psi(\chi_\rho(\widehat{x}))$. In fact, after rearranging (5), we have

$$\frac{\psi(\chi_\rho(\widehat{x})) - \psi(\chi)}{f(\rho)} = T_D\psi(\widehat{x}) + \frac{o(f(\rho))}{f(\rho)} \,. \tag{6}$$

Taking the limit $\rho \to 0^+$ in the above expression,

$$T_D\psi(\widehat{x}) = \lim_{\rho\to 0^+} \frac{\psi(\chi_\rho(\widehat{x})) - \psi(\chi)}{f(\rho)} \,. \tag{7}$$

Note that, the shape functionals $\psi(\chi_\rho(\widehat{x}))$ and $\psi(\chi)$ are associated to domains with different topologies. Then, to calculate the limit $\rho \to 0^+$ in (7) it is necessary to perform an asymptotic expansion of the functional $\psi(\chi_\rho(\widehat{x}))$ with respect to the parameter ρ.

Expression (7) represents the topological sensitivity of the shape functional $\psi(\chi)$ due to the introduction of a singular perturbation in an arbitrary point $\widehat{x} \in \Omega$. Historically, the topological derivative concept was rigorously introduced by Sokołowski and Żochowski (1999). Since then this concept has been widely used in several research areas and engineering applications, see for instance the works by Hintermüller and Laurain (2009), Hintermüller et al. (2012), Amstutz et al. (2012), Giusti et al. (2009, 2010b), Van Goethem and Novotny (2010) and Allaire et al. (2011) and the book by Novotny and Sokołowski (2013). In particular, for the mathematical analysis related to the fully coupled piezoelectric problem see Cardone et al. (2010). In particular, in this work, the topological derivative (7) will be used

as a feasible descent direction in a computational framework for topology optimization.

4 Topology optimization problem formulation

In order to design the piezoresistive devices, we propose the following multi-objective cost function:

$$\psi(\chi) := \mathcal{J}_\chi(\varphi,\phi) = (1-\omega)\mathcal{J}_{2\chi}(\varphi,\phi) - \omega\mathcal{J}_{1\chi}(\varphi,\phi)\ , \quad (8)$$

where ω is a weighting coefficient such that $0 \leq \omega \leq 1$, which allows control of the contribution between the functional $\mathcal{J}_{1\chi}(\varphi,\phi)$ and $\mathcal{J}_{2\chi}(\varphi,\phi)$; and the functional $\mathcal{J}_{1\chi}(\varphi,\phi)$ and $\mathcal{J}_{2\chi}(\varphi,\phi)$ are given by:

$$\mathcal{J}_{1\chi}(\varphi,\phi) := \int_\Omega (\varphi-\phi)^2\, d\Omega\ , \quad (9)$$

$$\mathcal{J}_{2\chi}(\varphi,\phi) := \frac{1}{2}\int_\Omega \bar{K}\nabla\phi\cdot\nabla\phi\, d\Omega\ . \quad (10)$$

The functional $\mathcal{J}_{1\chi}(\varphi,\phi)$ quantifies the sensitivity of the sensor. In other words, it measures the difference between the electric fields ϕ and φ on the piezoresistive membrane, i.e., the fields obtained when some force system is applied to the plate where the membrane is attached, and when no force is applied, respectively. The objective here is to maximize the sensitivity of the sensor. The functional $\mathcal{J}_{2\chi}(\varphi,\phi)$, on the other hand, is the inner electric energy associated to the piezoresistive problem (see (3)). This functional is added to stabilize the global behavior of the algorithm that minimizes the cost function $\mathcal{J}_\chi(\varphi,\phi)$.

In our particular case, we consider a singular perturbation in the domain given by the nucleation of a small circular inclusion $B_\rho(\hat{x})$ (see Fig. 3) with electric conductivity property γK. Here the parameter $\gamma \in [0,\infty)$ represents the contrast in the material property. Then, the constitutive properties in the perturbed configuration for problems (1) and (3) are, respectively, given by

$$\begin{cases} K & \text{if } x \in \Omega\setminus\overline{B_\rho} \\ \gamma K & \text{if } x \in B_\rho \end{cases} \text{ and } \begin{cases} \bar{K} & \text{if } x \in \Omega\setminus\overline{B_\rho} \\ \gamma\bar{K} & \text{if } x \in B_\rho \end{cases}\ . \quad (11)$$

Now, for an explicit and analytical formula for the topological derivative of the functional (8), when a singular perturbation as described above is inserted at an arbitrary point $\widehat{x}$, we introduce the following result:

Theorem 1 *For the shape functional stated in (8) and considering a disc of material characterized by the parameter γ – as topological perturbation – the analytical expression of the topological derivative (7) is given by:*

$$T_D\mathcal{J}_\chi(\widehat{x}) = (1-\omega)\, T_D\mathcal{J}_{2\chi}(\widehat{x}) - \omega\, T_D\mathcal{J}_{1\chi}(\widehat{x}) \qquad \forall \widehat{x}\in\Omega\ , \quad (12)$$

where $T_D\mathcal{J}_{1\chi}$ and $T_D\mathcal{J}_{2\chi}$ are scalar values at point $\widehat{x}$ given by:

$$T_D\mathcal{J}_{1\chi}(\widehat{x}) = 2\frac{1-\gamma}{1+\gamma}K\nabla\varphi(\widehat{x})\cdot\nabla p(\widehat{x}) + 2R^\top T R\nabla\phi(\widehat{x})\cdot\nabla q(\widehat{x})\ , \quad (13)$$

$$T_D\mathcal{J}_{2\chi}(\widehat{x}) = -R^\top T R\nabla\phi(\widehat{x})\cdot\nabla\phi(\widehat{x})\ , \quad (14)$$

where $\varphi(\widehat{x})$, $\phi(\widehat{x})$ are the solutions of the problems (1) and (3) in the unperturbed domain Ω at point $\widehat{x}$; and the matrix T is given by:

$$T = \sqrt{\det(\widetilde{K}(\widehat{x}))}\,\widetilde{K}(\widehat{x})S(\widehat{x}), \quad (15)$$

being $\widetilde{K}(\widehat{x})$ the diagonal representation of the tensor $\bar{K}$ at the point $\widehat{x}$, with eigenvalues k_1 and k_2, the matrix $S(\widehat{x})$ depending on the coefficients $\alpha = 1/\sqrt{k_1}$ and $\beta = 1/\sqrt{k_2}$, that is

$$S(\widehat{x}) = \frac{1}{2}(1-\gamma)\alpha\beta\begin{pmatrix} \frac{\alpha+\beta}{\alpha+\gamma\beta} & 0 \\ 0 & \frac{\alpha+\beta}{\beta+\gamma\alpha}\end{pmatrix} \quad (16)$$

and R is the rotation matrix that diagonalizes the tensor $\bar{K}$ at the point $\widehat{x}$. Finally, the functions $p(\widehat{x})$ and $q(\widehat{x})$ are the solutions of the following problems at the point $\widehat{x}$: find the functions $(p,q)\in\mathcal{V}\times\mathcal{V}$, such that:

$$\int_\Omega K\nabla p\cdot\nabla\eta\, d\Omega = 2\int_\Omega(\varphi-\phi)\eta\, d\Omega \quad \forall\eta\in\mathcal{V}\ , \quad (17)$$

$$\int_\Omega \bar{K}\nabla q\cdot\nabla\eta\, d\Omega = -2\int_\Omega(\varphi-\phi)\eta\, d\Omega \quad \forall\eta\in\mathcal{V}\ . \quad (18)$$

Proof The reader interested in the proof of this result may refer to Amstutz (2006), Giusti et al. (2010a) and Giusti and Novotny (2012). □

In this work, the topology of the substrate plate of the piezoresistive device is kept fixed, and the objective is to find the topology of the piezoresistive membrane (over the plate) that minimizes the multi-objective cost function (8), subjected to a volume constraint.

The optimization procedure is based on representing the domain in a bi-material fashion. The topology is identified by the strong material distribution (denoted as Ω^h) and the inclusions of weak material (denoted as Ω^s) are used to mimic the holes. The constitutive properties of these regions are characterized by the conductivity tensors K, $\bar{K}$ and the phase contrast γ^* so that, as in (11), we have

$$K(x) = \begin{cases} K & \forall x\in\Omega^h \\ \gamma^* K & \forall x\in\Omega^s \end{cases} \quad \text{and}$$

$$\bar{K}(x) = \begin{cases} K(I-\pi\sigma) & \forall x\in\Omega^h \\ \gamma^* K(I-\pi\sigma) & \forall x\in\Omega^s \end{cases}\ . \quad (19)$$

Based on the approach presented above, note that the constitutive properties of the domains Ω^h and Ω^s are correlated with the contrast parameter γ^* (see Fig. 4).

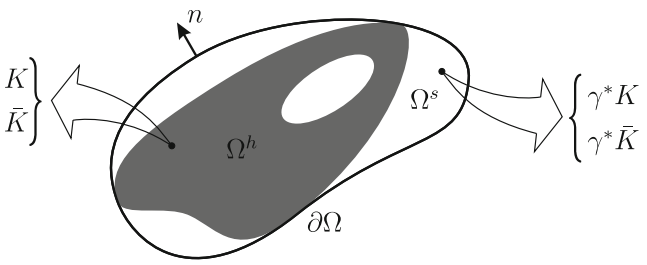

Fig. 4 Bi-material distribution in the domain Ω

A general optimization problem with a volume constraint can be stated as:

$$\begin{cases} \text{Minimize} & \psi(\chi) = \mathcal{J}_\chi, \\ \text{Subjected to} & |\Omega^h| = V^*, \end{cases} \tag{20}$$

where $|\Omega^h|$ is the Lebesgue measure of the domain Ω^h and V^* is the required volume at the end of the optimization process. In order to solve the above problem, we use an exact quadratic penalization scheme. Thus, problem (20) is re-written as following:

$$\underset{\Omega^h \subset \Omega}{\text{Minimize}}\ \mathcal{F}_\chi = \mathcal{J}_\chi + \lambda\, s_\chi^2, \tag{21}$$

being $\lambda > 0$ a Lagrange multiplier and the function s_χ is defined as

$$s_\chi := 1 - \frac{|\Omega^h|}{V^*}. \tag{22}$$

It should be stressed that the design variable in problem (21) is the topology of the domain Ω^h. Hence, by considering the exact topological sensitivity information provided by the topological derivative (12) it is possible to construct a numerical optimization procedure to tackle the problem. In this context and by considering the linearity property of the topological derivative operator, we see that the topological derivative of the cost function $\mathcal{F}_\chi$ presented in (21) is given by,

$$T_D\mathcal{F}_\chi = T_D\mathcal{J}_\chi + \lambda\, T_D s_\chi\,. \tag{23}$$

where $T_D\mathcal{J}_\chi$ is the topological derivative presented in (12) and $T_D s_\chi$ is the topological derivative of the function associated to the volume constraint s_χ, see Campeão et al. (2013), given by

$$T_D s_\chi = \begin{cases} -\frac{2}{V^*} s_\chi & \forall x \in \Omega^h \\ +\frac{2}{V^*} s_\chi & \forall x \in \Omega^s \end{cases}. \tag{24}$$

Note that the value of the parameter λ remains fixed in the optimization procedure, however the value of the function s_χ must be updated at each step.

From the definition of the conductivity piezoresistive tensor (19), we remark that (23) always measures the sensitivity of $\mathcal{F}_\chi$ when the two materials are interchanged within the domain. Then, the computation of (23) is carried out by using the expressions (12)–(16) with $\gamma = \gamma^*$ if $x \in \Omega^h$; and $\gamma = 1/\gamma^*$ if $x \in \Omega^s$. Having made the previous consideration and in order to solve the optimization problem (21), we use the topology optimization algorithm proposed by Amstutz and Andrä (2006). The procedure relies on a level-set domain representation (Osher and Sethian 1988) and the approximation of the topological optimality conditions by a fixed point iteration. The topological derivative (23) is used as a feasible descent direction to minimize the cost function $\mathcal{F}_\chi$. This class of algorithm has been successfully used in research areas related to topological optimization such as: microstructure of materials (Amstutz et al. 2010), load bearing structures and flow through porous media (Amstutz and Andrä 2006), load bearing structures subjected to pointwise stress constraint (Amstutz and Novotny 2010; Amstutz et al. 2012) and thermal conductors in anisotropic medium Giusti and Novotny (2012). For completeness, the algorithm is outlined in the following. For further details we refer to the work by Amstutz and Andrä (2006) and Amstutz et al. (2012).

By considering the level-set domain representation, the strong (or hard) material is characterized by a function $\Psi \in L^2(\Omega)$ such that

$$\Omega^h = \{x \in \Omega,\, \Psi(x) < 0\}\,, \tag{25}$$

whereas the weak (or soft) material domain is defined by

$$\Omega^s = \{x \in \Omega,\, \Psi(x) > 0\}\,. \tag{26}$$

Now, let us consider the topological derivative $T_D\mathcal{F}_\chi$. According to Amstutz and Andrä (2006), a sufficient condition of *local optimality* of problem (21) for the class of perturbations consisting of circular inclusions is

$$T_D\mathcal{F}_\chi(x) > 0 \quad \forall x \in \Omega\,. \tag{27}$$

To devise a level-set-based algorithm whose aim is to produce a topology that satisfies (27) it is convenient to define the function

$$g(x) = \begin{cases} -T_D^h\mathcal{F}_\chi(x) & \text{if } x \in \Omega^h \\ T_D^s\mathcal{F}_\chi(x) & \text{if } x \in \Omega^s \end{cases}. \tag{28}$$

With the above definition and (25), (26) it can be easily established that the sufficient condition (27) is satisfied if the following equivalence relation between the functions g and the level-set Ψ holds

$$\exists\, \tau > 0 \quad \text{s.t} \quad g = \tau\, \Psi\,, \tag{29}$$

or, equivalently,

$$\theta := \arccos\left[\frac{\langle g, \Psi\rangle_{L^2(\Omega)}}{\|g\|_{L^2(\Omega)}\, \|\Psi\|_{L^2(\Omega)}}\right] = 0\,, \tag{30}$$

where θ is the angle between the vectors g and Ψ in $L^2(\Omega)$. Starting from a given level-set function $\Psi_0 \in L^2(\Omega)$ which defines the chosen initial guess for the optimum topology, the algorithm proposed by Amstutz and Andrä (2006)

produces a sequence $(\Psi_i)_{i\in\mathbb{N}}$ of level-set functions that provides successive approximations to the sufficient condition for optimality (29). The sequence satisfies

$$\begin{aligned} &\Psi_0 \in L^2(\Omega)\ , \\ &\Psi_{i+1} \in \mathrm{co}(\Psi_i, g_i) \qquad \forall i \in \mathbb{N}\ , \end{aligned} \tag{31}$$

where $\mathrm{co}(\Psi_i, g_i)$ is the convex hull of $\{\Psi_i, g_i\}$. In the current algorithm the initial guess Ψ_0 is normalized. With $\mathcal{S}$ denoting the unit sphere in $L^2(\Omega)$, the algorithm is explicitly given by

$$\begin{aligned} &\Psi_0 \in \mathcal{S}\ , \\ &\Psi_{i+1} = \frac{1}{\sin\theta_i}\left[\sin((1-\kappa_i)\theta_i)\Psi_i + \sin(\kappa_i\theta_i)\frac{g_i}{\|g_i\|_{L^2(\Omega)}}\right], \end{aligned} \tag{32}$$

where $\kappa_i \in [0, 1]$ is a step size determined by a line-search in order to decrease the value of the cost functional $\mathcal{F}_\chi$. The iterative process is stopped when for some iteration the obtained decrease in $\mathcal{F}_\chi$ is smaller than a given numerical tolerance. If, at this stage, the optimality condition (29), (30) is not satisfied to the desired degree of accuracy, i.e. if $\theta_{i+1} > \epsilon_\theta$, where ϵ_θ is a pre-specified convergence tolerance, then a uniform mesh refinement of the structure is carried out and the procedure is continued.

Based on the above description, the main steps of the algorithm can be summarized as following:

1. Choose an initial level-set function by defining the initial guess for the design domain;
2. Define the domains Ω^h and Ω^s according to (25) and (26);
3. Define the constitutive properties for the finite elements in each domain Ω^h and Ω^s according to (19);
4. Obtain the discretized fields ϕ, φ, p and q by solving, respectively, the problems (1) and (3); and the adjoint equations (17) and (18) by using the standard FEM;
5. Compute the topological derivative field (12) at Gauss point of the finite element and perform a standard nodal averaging procedure;
6. Obtain the function $g(x)$ according to (28) by using the nodal values of the topological derivative and compute the θ angle with (30);
7. Update the level-set function Ψ_{i+1} according to (32) and update the domains Ω^h and Ω^s by considering eqs. (25) and (26);
8. Check convergence $\theta_{i+1} \leq \epsilon_\theta$. If True: Exit. If False: goto 3.

A general flowchart for the algorithm is shown in Fig. 5.

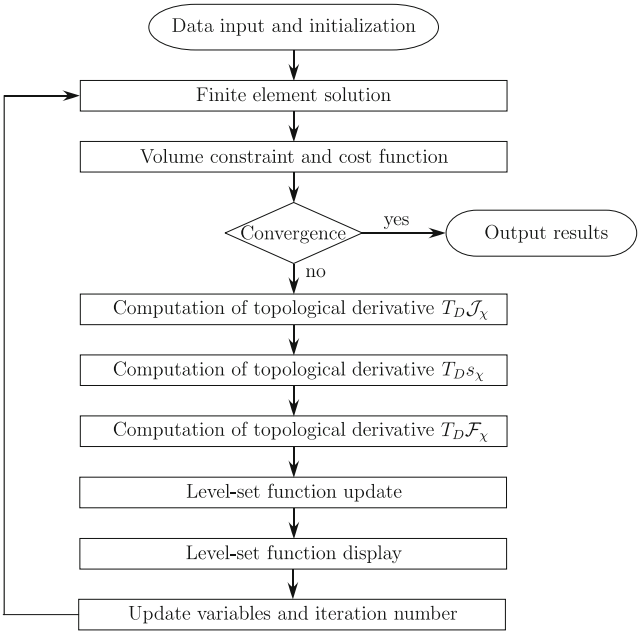

Fig. 5 Flowchart of the optimization algorithm

5 Numerical examples

To illustrate the applicability of expression (23) and the optimization procedure presented in the previous Section, we present four numerical examples considering different volume constraint and distinct boundary conditions in the conductivity problem. As mentioned before, the optimized distribution of piezoresistive material over a base plate is obtained. In the figures of results, the black part represents the domain Ω^h and the white part is Ω^s.

In all examples, the base plate is given by a square domain $(0, 1.0) \times (0, 1.0)m$, whose boundaries remain fixed (see Fig. 6, where the thick lines represent clamped boundary conditions). The plate is submitted to an uniform pressure of $10000N/m^2$, and it is made of aluminum, with parameters Young's modulus and Poisson's ratio equal to $80GPa$ and 0.33, respectively. The plate problem is solved using the DKT finite element (Discrete Kirchhoff Triangle), see the work by Batoz (1982). The domain, load and boundary condition for the plate (substrate) problem are depicted in Fig. 6.

For computational implementation purpose, we adopt the matrix representation of the fourth-order elasticity tensor $\mathbb{C}$, denoted as D (3×3 matrix in 2D). The constitutive properties of the piezoresistive material (n–Si) are presented in Table 1, where D_{ij} are the components of the elasticity matrix D. For the computation of the topological derivative, we consider the value of the contrast parameter given by $\gamma^* = 10^{-4}$. The initial guess for the optimization of the piezoresistive membrane (over the plate) is the fully covered

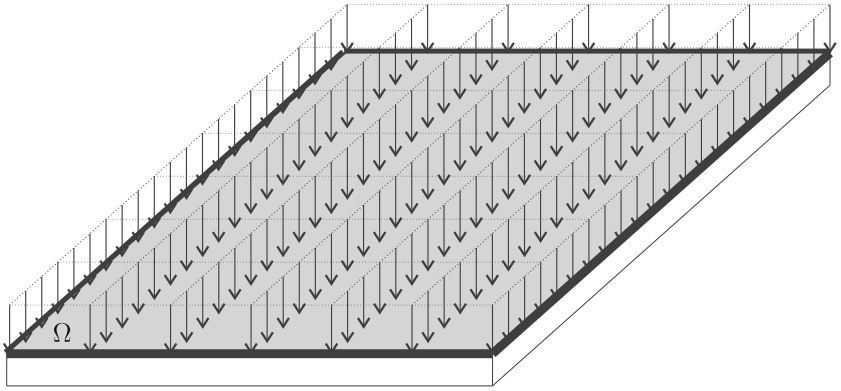

Fig. 6 Numerical examples. Domain, load and boundary conditions for the substrate

domain. To ensure that the obtained results satisfy the optimality condition (30), in all the examples it is considered a convergence tolerance $\epsilon_\theta = 3°$.

5.1 Example 1

For this first example, the boundary conditions are prescribed in small regions Γ_{D_1} and Γ_{D_2}, where the values are $\bar{\varphi}|_{\Gamma_{D_1}} = 50V$ and $\bar{\varphi}|_{\Gamma_{D_2}} = 0V$, respectively. The domain and boundary conditions for this example are shown in Fig. 7, where $a = 0.2m$. The volume constraint is chosen to be 30 % of the design domain. The optimized topologies for the membrane, with different values of the weighting coefficient ω, are shown in Fig. 8.

We are interested in studying the stability of this methodology with respect to the prescribed volume fraction. Therefore, we repeat the optimization procedure described above with different values of the parameter V^*. In particular, we set the volume constraint to 10 % and 5 % of the initial volume. The obtained results for the optimized topology of the piezoresistive membrane are shown in Figs. 9 and 10, for three different values of the weighting coefficient ω. These results show that the proposed approach works even for such a severe constraint.

For the volume fractions and the set of parameters ω studied, the optimized topology is characterized by a strip of piezoresistive material over the square plate. The strip connects the Dirichlet data in the opposite sides of the plate, and its width and shape depends on the required final volume fraction V^* and weighting coefficient ω.

Table 1 Constitutive properties of n-Si

k	π_{11}	π_{12}	π_{44}
$(\Omega.m)^{-1}$	$(10^{-11}m^2/N)$	$(10^{-11}m^2/N)$	$(10^{-11}m^2/N)$
1/0.117	−102.2	53.4	−13.6
	D_{11}	D_{12}	D_{44}
	(GPa)	(GPa)	(GPa)
	165.7	63.9	79.6

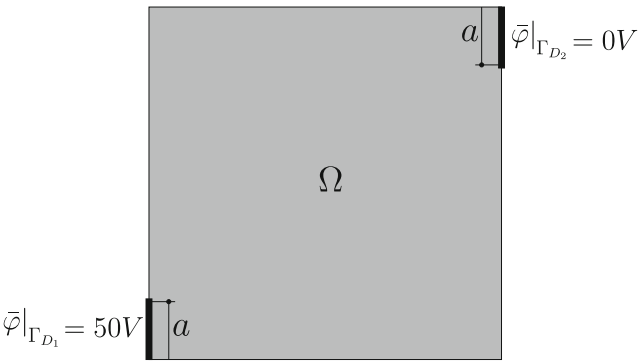

Fig. 7 Example 1. Domain and boundary conditions for the membrane

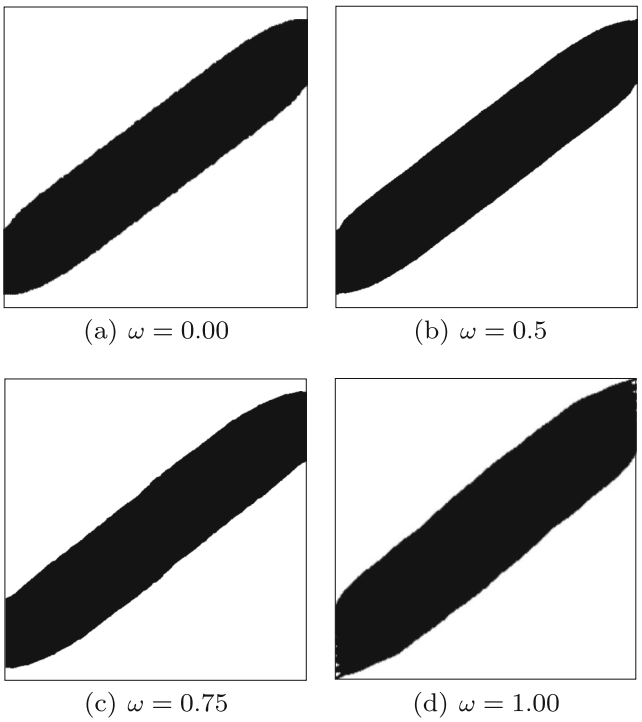

Fig. 8 Example 1. Results for 30 % of volume fraction

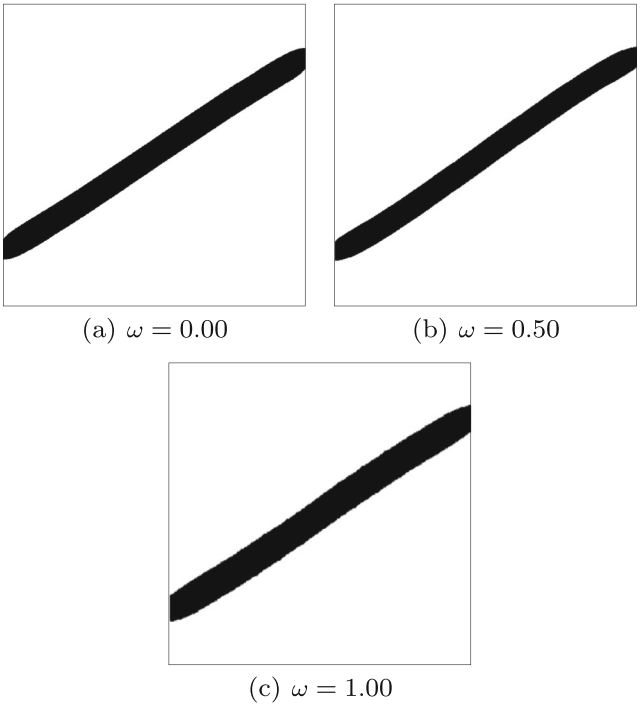

(a) $\omega = 0.00$ (b) $\omega = 0.50$

(c) $\omega = 1.00$

Fig. 9 Example 1. Results for 10 % of volume fraction

In order to analyze the results from a quantitative point of view, in Table 2 we present, for each set of parameters V^* and ω, the obtained improvement in the sensor response (functional $\mathcal{J}_{1\chi}$), i.e., the percentage difference between the functional values for the initial guess and the obtained result (Imp [%] := $\frac{\mathcal{J}_{1\chi}|_{opt}}{\mathcal{J}_{1\chi}|_{ini}} - 1$). These results show that optimized topologies with a improvement value of the functional $\mathcal{J}_{1\chi}$ equal to 106 % (mean value) can be obtained with only 5 % of piezoresistive material. Moreover, for 30 % of piezoresistive material, the improvement in the functional $\mathcal{J}_{1\chi}$ is around to 77 % (mean value). In addition, to establish a comparison of the obtained designs in relation to each other, it is presented in Table 2 the ratio between the normalized value of the functional $\mathcal{J}_{1\chi}$ and the same value obtained for the case $\omega = 0$, i.e. $\alpha_\omega = \frac{\mathcal{J}_{1\chi}}{\mathcal{J}_{1\chi}|_{\omega=0}}$. The results presented here, specially for the smaller volume fractions, clearly show the stabilization effect of the functional $\mathcal{J}_{2\chi}$ (see (8) and (10)), which favours smooth boundaries and takes less iterations to converge without affecting significatively the improvement in the sensor response. From Table 2, it follows straightforward that it exists an optimized volume whose improvement in the sensor response is better. In Fig. 11 it is shown the improvement values vs. the volume constraint V^* for three different weighting coefficient ω. From this figure it is clear that the optimized volume constraint is close to 10 % of the initial volume.

Table 2 Example 1. Improvement in the sensor response

V^*	30 %		
ω	0.00	0.50	1.00
$\mathcal{J}_{1\chi}$	0.03148	0.03149	0.03189
$\mathcal{J}_{2\chi}$	4.66×10^5	9.32×10^5	9.50×10^5
Imp.	75.9 %	76.0 %	78.2 %
α_ω	1.000	1.000	1.013
Iter.	63	90	125
V^*	10 %		
ω	0.00	0.50	1.00
$\mathcal{J}_{1\chi}$	0.0363	0.0367	0.0378
$\mathcal{J}_{2\chi}$	2.44×10^5	2.59×10^5	2.68×10^5
Imp.	102 %	104 %	110 %
α_ω	1.000	1.009	1.041
Iter.	128	136	240
V^*	5 %		
ω	0.00	0.50	1.00
$\mathcal{J}_{1\chi}$	0.0359	0.0361	0.0362
$\mathcal{J}_{2\chi}$	1.64×10^5	1.64×10^5	3.23×10^5
Imp.	100.01 %	100.66 %	101.69 %
α_ω	1.000	1.003	1.007
Iter.	240	240	290

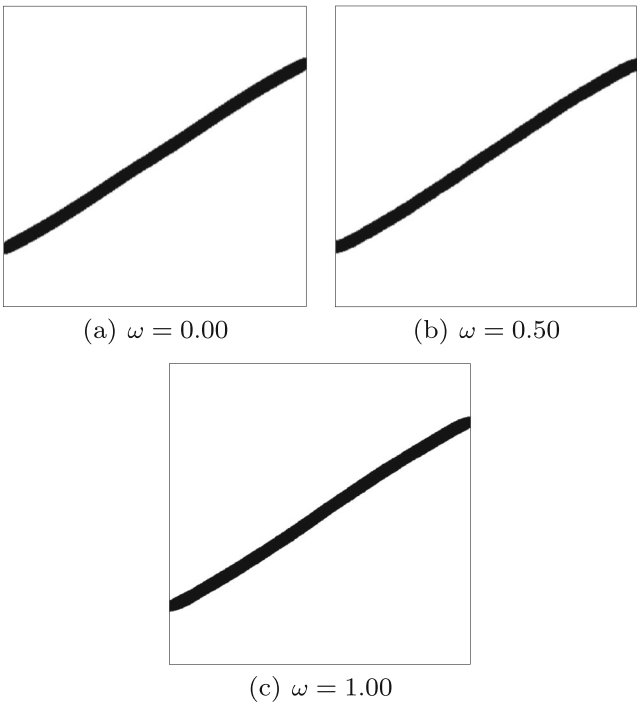

(a) $\omega = 0.00$ (b) $\omega = 0.50$

(c) $\omega = 1.00$

Fig. 10 Example 1. Results for 5 % of volume fraction

5.2 Example 2

For this example the boundary conditions are prescribed in three points namely Γ_{D_1}, Γ_{D_2} and Γ_{D_3}, where the values are

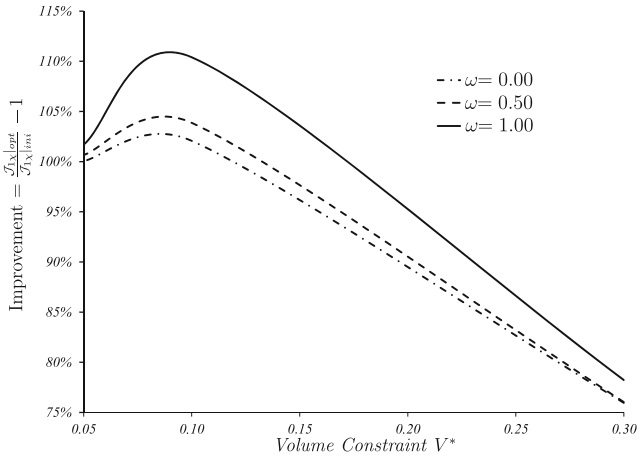

Fig. 11 Example 1. Optimized volume constraint value

$\bar{\varphi}|_{\Gamma_{D_1}} = 50V$, $\bar{\varphi}|_{\Gamma_{D_2}} = 0V$ and $\bar{\varphi}|_{\Gamma_{D_3}} = 0V$. The domain and boundary conditions for this example are shown in Fig. 12, where $a = 0.25m$. The volume constraint is chosen to be 20 % of the initial volume. The optimized topologies for the piezoresistive material are shown in Fig. 13, for different values of the weighting coefficient ω.

From these results, the optimized distribution of piezoresistive material over the substrate is a strip connecting the three points where the Dirichlet data are prescribed. For all values of the parameter ω studied in this example, the topology is essentially the same. The influence of ω is only manifested in the shape of the membrane. In the same way as before, in Table 3, we present the improvement of the sensor response w.r.t. the initial guess, the values of the parameter α_ω defined earlier and the iterations needed to converge. The obtained improvements in the value of the cost functional $\mathcal{J}_{1\chi}$, for this particular example, are about 106 % (average of values shown in Table 3).

5.3 Example 3

The Dirichlet boundary conditions for this example are prescribed in four points, namely Γ_{D_1}, Γ_{D_2}, Γ_{D_3} and Γ_{D_4}; where the values are $\bar{\varphi}|_{\Gamma_{D_1}} = 50V$, $\bar{\varphi}|_{\Gamma_{D_2}} = 0V$, $\bar{\varphi}|_{\Gamma_{D_3}} = 0V$ and $\bar{\varphi}|_{\Gamma_{D_4}} = 25V$. The domain and boundary conditions for this example are shown in Fig. 14, where $a = 0.25m$ and $b = 0.125m$. The volume constraint is chosen to be 30 % of the initial volume. The iterations needed to solve this problem are presented in Table 4.

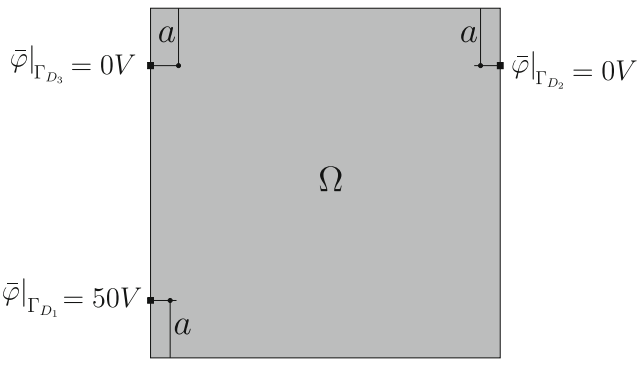

Fig. 12 Example 2. Domain and boundary conditions for the membrane

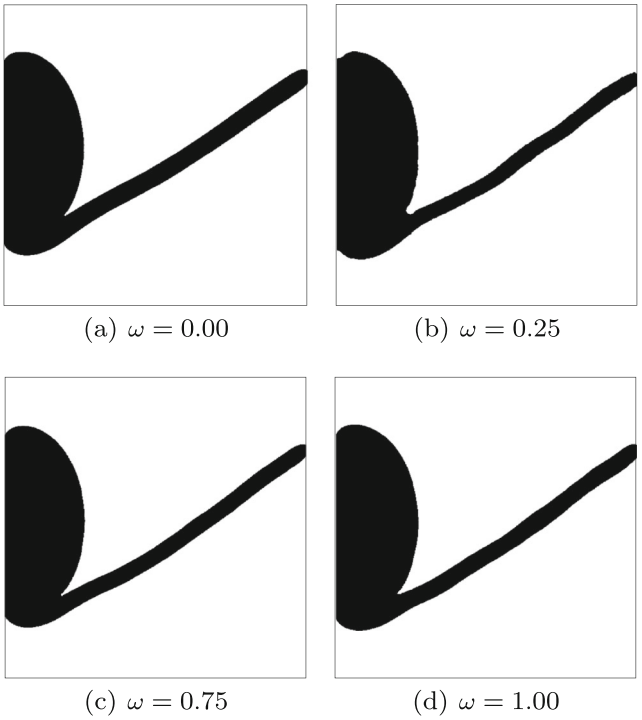

Fig. 13 Example 2. Results for 20 % of volume fraction

The optimized topologies for the piezoresistive membrane are shown in Fig. 15, for different values of the weighting coefficient ω. Once again, these results clearly show the stabilization effect of the functional $\mathcal{J}_{2\chi}$ (see (8) and (10)), which favours smooth boundaries. Also, the number of iteration needed by the algorithm to converge is smaller for $\omega = 0.00$.

Table 4 presents the percentage improvements of the shape functional $\mathcal{J}_{1\chi}(\varphi, \phi)$ (once again, optimized results are compared against the initial guess). Also, the values of the coefficient α_ω are shown in the same Table. Improvements of up to 83 % are obtained (average of values shown in Table 4).

Table 3 Example 2. Improvement in the sensor response

V^*	20%			
ω	0.00	0.25	0.75	1.00
$\mathcal{J}_{1\chi}$	0.0594	0.0605	0.0612	0.0615
$\mathcal{J}_{2\chi}$	1.911×10^4	1.914×10^4	1.913×10^4	1.928×10^4
Imp.	102 %	106 %	108 %	109 %
α_ω	1.000	1.020	1.030	1.035
Iter.	50	40	44	90

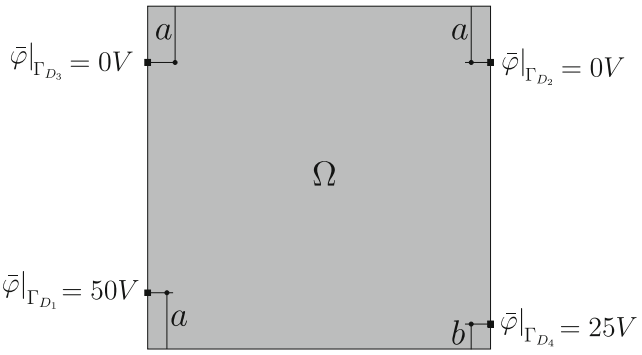

Fig. 14 Example 3. Domain and boundary conditions for the membrane

On the other hand, it is interesting to note the change in the final topology. In fact, the topologies for $\omega \in \{0.00, 0.25\}$ and $\omega \in \{0.75, 1.00\}$ are different, see Fig. 15. The change appears for values of ω between 0.73 and 0.74, as it can be seen in Fig. 16. However, the change in the topology does not affect the behavior of the sensor significantly, see results from Table 4. This fact suggests that the optimization problem for this example has local minima. Finally, note that for values of ω greater than 0.74 the results seem to indicate that the connection of the sensor in the point 4 (Γ_{D_4}) is no more necessary, i.e. the maximization of the potential difference is obtained only with three connections.

5.4 Example 4

In this last example, we use a similar configuration to the previous example for the points where the Dirichlet boundary conditions are prescribed. In particular, we use four points where the values are $\bar{\varphi}|_{\Gamma_{D_1}} = \bar{\varphi}|_{\Gamma_{D_2}} = 50V$ and $\bar{\varphi}|_{\Gamma_{D_3}} = \bar{\varphi}|_{\Gamma_{D_4}} = 25V$. The domain and boundary conditions for this example are shown in Fig. 17, where $a = 0.25m$. The optimization procedure is applied for different values of volume constraint V^*. By considering the results of the previous examples, here only the case $\omega = 1.00$ is considered. The obtained topologies are presented in Fig. 18 and the improvement values of the sensor are shown in Table 5.

Table 4 Example 3. Improvement in the sensor response

V^*	30 %			
ω	0.00	0.25	0.75	1.00
$\mathcal{J}_{1\chi}$	0.0586	0.0597	0.0601	0.0604
$\mathcal{J}_{2\chi}$	1.88×10^4	1.89×10^4	1.93×10^4	1.95×10^4
Imp.	80 %	84 %	85 %	86 %
α_ω	1.000	1.020	1.025	1.032
Iter.	40	57	47	72
V^*	30 %			
ω	0.73	0.74		
$\mathcal{J}_{1\chi}$	0.0598	0.0598		
$\mathcal{J}_{2\chi}$	1.91×10^4	1.92×10^4		
Imp.	84 %	84 %		
α_ω	1.021	1.021		

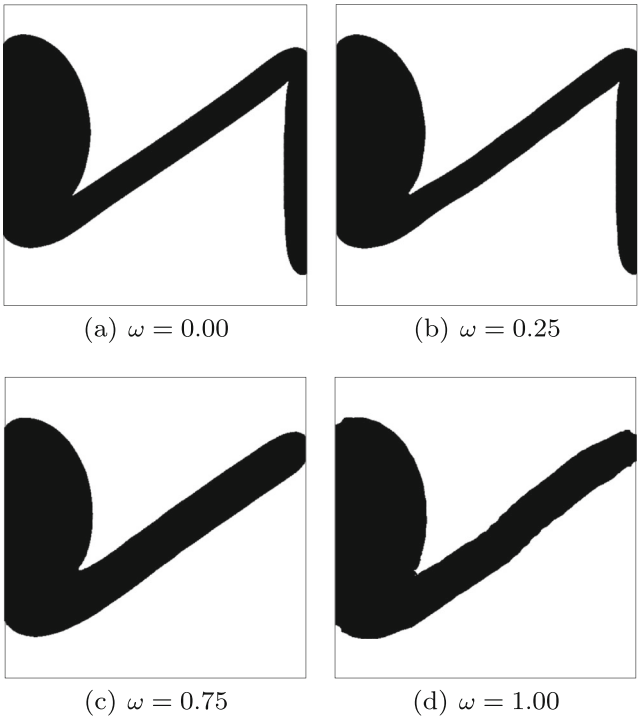

Fig. 15 Example 3. Results for 30 % of volume fraction

The optimized topology for the membrane is characterized by two blocks of piezoresistive material, each one connecting the two points Γ_D in each side; and two strips connecting both sides of the sensor. Initially, the algorithm creates a hole in the center of the design domain and after it develops the shapes of the strips. This configuration is obtained independently of the volume constraint. For each value of V^* the optimized topology is the same and only

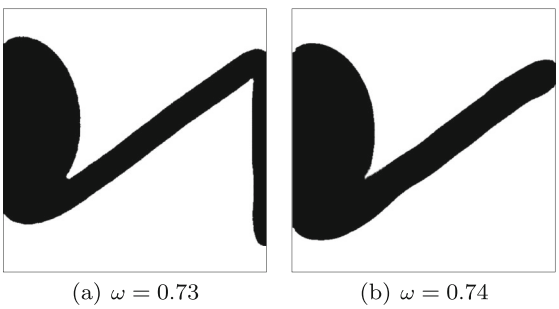

Fig. 16 Example 3. Change in the final topology

changes in the shapes are manifested, as it can be seen in Fig. 18. By applying the technique described in Example 1, the optimized volume of the piezoresistive membrane that maximizes the sensor response is close to the 40 % of the initial volume. In Fig. 19, the improvement values of the optimized topologies vs. the volume constraint are presented.

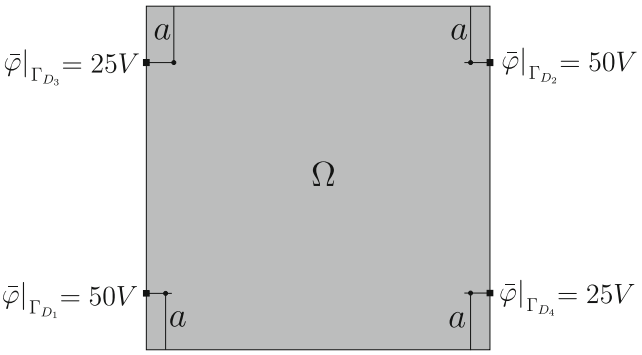

Fig. 17 Example 4. Domain and boundary conditions for the membrane

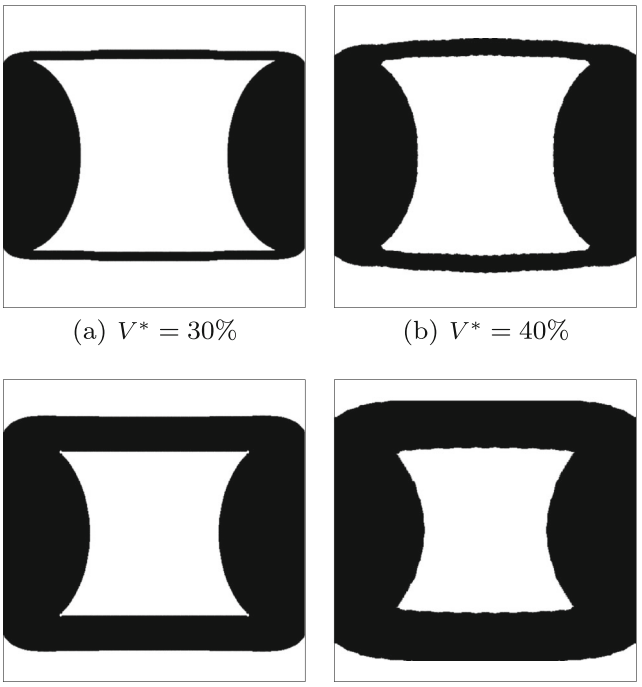

Fig. 18 Example 4. Results for $\omega = 1.00$

Table 5 Example 4. Improvement in the sensor response

ω	1.00			
V^*	30 %	40 %	50 %	60 %
$\mathcal{J}_{1\chi}$	0.0145	0.0147	0.0140	0.0109
Imp.	170 %	173 %	160 %	102 %
α_ω	1.000	1.012	0.962	0.749
Iter.	150	81	91	86

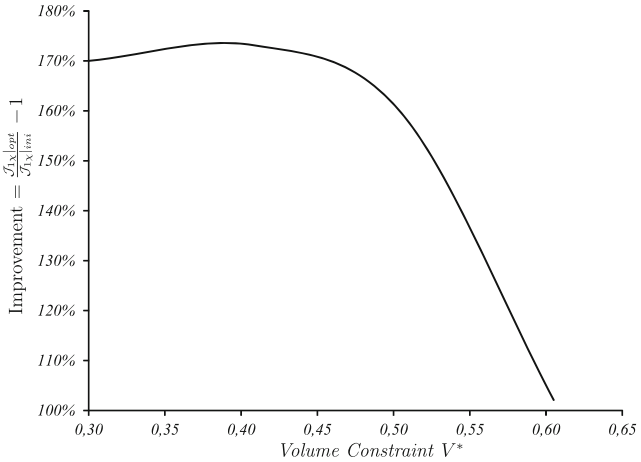

Fig. 19 Example 4. Optimized volume constraint value

6 Conclusion and extension

In this work, the applicability of the topological derivative concept to a piezoresistive sensor design has been successfully presented. An analytical expression for the topological derivative has been implemented in a topological design algorithm based on a level-set domain representation method. The final formula is a general simple analytical expression in terms of the solution of the state equation and the constitutive parameters evaluated at each point of the domain. This derivative is used as a feasible descent direction in a topology design algorithm. Four numerical experiments associated to the topology optimization of the piezoresistive membrane of a pressure sensor are presented. The efficiency and stability of the methodology presented in this work has been studied in the numerical examples. The results show an improvement in the sensor response of around 75 % to 110 % (depending on the boundary condition and volume constraint employed) in relation to a fully covered sensor. Relative to the optimized volume, with this methodology it is possible to find the optimized volume after some realizations. This characteristic of the proposed method is shown in the numerical examples, where it is clear that exists a volume of piezoresistive material whose improvement is better (see Examples 1 and 4). In general, the influence of the weighting coefficient ω is manifested in the shape of the optimized membrane. However, in one example, the obtained topology depends on the value of the weighting coefficient ω, see Figs. 15 and 16, without affecting significatively the improvement of the sensor response. The obtained results in the numerical examples

clearly show the stabilization effect of the functional $\mathcal{J}_{2\chi}$. The addition of this functional to the objective functional $\mathcal{J}_\chi$ allow obtaining smooth shapes for the membrane, reducing the number of iterations to converge and requiring a finite element mesh with less elements. However, the best improvement value in each numerical example is obtained for $\omega = 1.00$. This indicates that exists a trade-off between the *best result* and the *computational cost* to solve the optimization problem by using the methodology presented in this work. As an extension of this work, the authors intend to compare the proposed approach with other approaches, such as the described in Pedersen (2004), Rubio et al. (2008) and Mello et al. (2012), for instance.

Acknowledgments This research was partially supported by PRONEX-FAPERJ (n.^{o} E-26/110.561/2010) programme (Brazil), CNPq (National Council for Scientific and Technological Development, CONICET (National Council for Scientific and Technical Research, Argentina) and PID-UTN (Research and Development Program of the National Technological University, Argentina). The supports of these agencies are gratefully acknowledged. More specifically, the last author is thankful for the financial support received from CNPq, $n.^o$ 304121/2013-4.

References

Allaire G, Jouve F, Van Goethem N (2011) Damage and fracture evolution in brittle materials by shape optimization methods. J Comput Phys 230(12):5010–5044

Amarasinghe R, Dao DV, Toriyama T, Sugiyama S (2005) Design and fabrication of a miniaturized six-degree-of-freedom piezoresistive accelerometer. J Micromech Microeng 15:1745–1753

Amstutz S (2006) Sensitivity analysis with respect to a local perturbation of the material property. Asymptot Anal 49(1-2):87–108

Amstutz S, Andrä H (2006) A new algorithm for topology optimization using a level-set method. J Comput Phys 216(2):573–588

Amstutz S, Novotny AA (2010) Topological optimization of structures subject to von Mises stress constraints. Struct Multidiscip Optim 41(3):407–420

Amstutz S, Giusti SM, Novotny AA, de Souza Neto EA (2010) Topological derivative for multi-scale linear elasticity models applied to the synthesis of microstructures. Int J Numer Methods Eng 84:733–756

Amstutz S, Novotny AA, de Souza Neto EA (2012) Topological derivative-based topology optimization of structures subject to Drucker-Prager stress constraints. Comput Methods Appl Mech Eng 233–236:123–136

Batoz JL (1982) An explicit formulation for an efficient triangular plate-bending element. Int J Numer Methods Eng 18:1077–1089

Buchhold R, Gollee R, Nakladal A, Gerlach G (2000) A novel approach to modeling the transfer functions of four-terminal-transducer pressure sensors within a single simulation tool. Sensors Actuators A Phys 80(1):15–22

Campeão DE, Giusti SM, Novotny AA (2013) Topology design of plates consedering different volume control methods. Engineering Computations To Appears

Cardone G, Nazarov S, Sokołowski J (2010) Asymptotic analysis, polarization matrices, and topological derivatives for piezoelectric materials with small voids. SIAM J Control Optim 48(6):3925–3961

Giusti SM, Novotny AA (2012) Topological derivative for an anisotropic and heterogeneous heat diffusion problem. Mech Res Commun 46:26–33

Giusti SM, Novotny AA, de Souza Neto EA, Feijóo RA (2009) Sensitivity of the macroscopic elasticity tensor to topological microstructural changes. J Mech Phys Solids 57(3):555–570

Giusti SM, Novotny AA, Sokołowski J (2010a) Topological derivative for steady-state orthotropic heat diffusion problem. Struct Multidiscip Optim 40(1):53–64

Giusti SM, Novotny AA, de Souza Neto EA (2010b) Sensitivity of the macroscopic response of elastic microstructures to the insertion of inclusions. Proc R Soc A Math Phys Eng Sci 466:1703–1723

Hintermüller M, Laurain A (2009) Multiphase image segmentation and modulation recovery based on shape and topological sensitivity. J Math Imaging Vis 35:1–22

Hintermüller M, Laurain A, Novotny AA (2012) Second-order topological expansion for electrical impedance tomography. Adv Comput Math 36(2):235–265

Hsieh MC, Fang YK, Ju MS, Chen GS, Ho JJ, Wu CHYPM, Wu GS, Chen TYF (2001) A contact-type piezoresistive micro-shear stress sensor for above-knee prosthesis application. J Microelectromech Syst 10:121–127

Mello LAM, Takezawa A, Silva ECN (2012) Designing piezoresistive plate-based sensors with distribution of piezoresistive material using topology optimization. Smart Mater Struct 21(8):085, 029

Mescheder U, Majer S (1997) Micromechanical inclinometer. Sensors Actuators A Phys 60(1–3):134–138

Novotny AA, Sokołowski J (2013) Topological derivatives in shape optimization. Interaction of Mechanics and Mathematics, Springer

Osher S, Sethian JA (1988) Front propagating with curvature dependent speed: algorithms based on hamilton-jacobi formulations. J Comput Phys 78:12–49

Pedersen NL (2004) On optimization of bio-probes. Int J Numer Methods Eng 61(6):791–806

Plaza JA, Esteves J, Cané C (2000) Twin-mass accelerometer optimization to reduce the package stresses. Sensors Actuators A Phys 80(3):199–207

Plaza JA, Collado A, Cabruja E, Esteves J (2002) Piezoresistive accelerometers for mcm package. J Microelectromech Syst 11(6):794–801

Rubio WM, Silva ECN, Nishiwaki S (2008) Piezoresistive sensor design using topology optimization. Struct Multidiscip Optim 36(6):571–583

Sokołowski J, Żochowski A (1999) On the topological derivative in shape optimization. SIAM J Control Optim 37(4):1251–1272

Sze SM (2000) Semiconductor sensors. Wiley, New York

Van Goethem N, Novotny AA (2010) Crack nucleation sensitivity analysis. Math Methods Appl Sci 33(16):197–1994

Wang F, Jensen JS, Sigmund O (2011) Robust topology optimization of photonic crystal waveguides with tailored dispersion properties. J Opt Soc Am B 28(3):387–397

Wang MY, Wang XM, Guo DM (2003) A level set method for structural topology optimization. Comput Methods Appl Mech Eng 192(1–2):227–246

Xiao J, Li Y, Fan WX (1999) A laminate theory of piezoresistance for composite laminates. Compos Sci Technol 59(9):1369–1373